QUANTITATIVE EVALUATION OF THE SHADING RESILIENCE OF PV MODULES

[1,2,*]Nils Klasen, [1]Florian Lux, [1]Julian Weber, [1]Daniel Weißer, [1]Torsten Roessler, [1]Achim Kraft, [1]Dirk Holger Neuhaus

[1] Fraunhofer Institute for Solar Energy Systems ISE
Heidenhofstraße 2, 79110 Freiburg i.Br., Germany

[2] Karlsruhe Institute of Technology KIT, Institute for Applied Materials – Material and Biomechanics (IAM-WBM)
Hermann-von-Helmholtz-Platz 1, 76344 Eggenstein-Leopoldshafen, Germany

[*]corresponding author, e-mail to: nils.klasen@ise.fraunhofer.de

ABSTRACT: We present simulation results on the partial shading behavior of four PV module layout containing three different solar cell sizes. Two types of shingle interconnection are compared to the widely used "butterfly" layout for half-cut solar cells and the conventional solar cell interconnection of 60 full size solar cells. For the LT spice simulations, we measured the *I-V* characteristic of PERC shingle solar cells and included the reverse breakdown region into an extended two-diode model. Two basic shading cases, rectangular and random shading, are investigated. Therefore, we created sets of > 1000 scenarios per case by Latin Hypercube Sampling (LHS). The scenarios are transferable for all solar cell sizes and the number of full solar cell equivalents identical in all topologies. We apply a new criterion [1] for evaluation of the shading resilience SR from 0 to 1 to compare and rank the different cell topologies regarding their performance under partial shading. The shading resilience for rectangular shadings of the shingle matrix layout ($SR = 0.692$) excels the one of the shingle string layout ($SR = 0.602, 87$ % of the matrix layout), the butterfly layout ($SR = 0.461, 67$ %) and the conventional full cell interconnection ($SR = 0.213, 31$ %) scheme. We find minor differences in the absolute values for random shading. However, the ranking of the solar modules stays identical. Finally, we conclude that besides higher power densities and a valuable aesthetical appearance, shingle solar modules feature an additional very important but so far little noticed and discussed property: Overall higher power outputs under partial shading. This makes them especially suited for vehicle and building integrated applications.

Keywords: Partial Shading, Shingle Solar Cell Interconnection, LTspice

1 INTRODUCTION

Shading of photovoltaic modules can cause severe losses in the output power of PV generators. In integrated applications such as buildings and cars this becomes especially relevant. U. Jahn and W. Nasse showed in early studies of roof top installations in Germany that 41 % of the installed systems were affected by shading and shading-related energy yield losses of up to 20 % [2]. C. Schuss *et al.* investigated the shading of car roofs due to vegetation during operation [3, 4]. Poles and antennas cause shading as well as shown in [5, 6]. From these two cases we derive two cases to be considered in this study: Random and rectangular shading of solar modules.

So far bypass-diodes are the established measure to reduce shading losses in PV solar modules. However, in recent years a variety of new interconnection technologies and solar cell geometries allow for another option of shading loss reduction: Adapted module layouts. When shading occurs, the current generation reduction in shaded solar cells and the resulting current mismatch with the unshaded cells is responsible for the loss in power. Parallel interconnection is the solution to avoid these losses since currents add up and current mismatch has no negative effect. However, there are limits to that due to ohmic loss reduction and the need of reasonable voltage levels. Adapted module layouts allow the combination of serial and parallel interconnections of the incorporated solar cells.

Half-cut and shingle solar cells allow the implementation of mixed interconnections while at the same time maintaining similar current-voltage levels compared to conventional full-cell topologies. We investigated four topologies based on full-sized, half-cut and shingle solar cells with respect to their shading resilience under random and rectangular shading. All four topologies are highly relevant for the application in commercial module products.

2 METHODOLOGY

2.1 *I-V* Characteristics

In this study, we use *I-V* characteristics obtained in previous work [7]. An extended two-diode model is used to describe the entire current-voltage curve including the reverse breakdown region. The exponential current increase during reverse breakdown is added to the known two-diode equivalent circuit by another Schottky diode term as proposed by H.S. Rauschenbach [8]. This Schottky diode term requires three additional fit parameters: The reverse breakdown saturation current density J_{Br}, an avalanche factor to be multiplied with the diode ideality factor n to form n_{Br} and a reverse breakdown voltage V_{Br}. Equation (1) describes the entire solar cell characteristic. For more detailed information on the measurement procedure and data obtained for lab-scale and commercial PERC shingle solar cells, we refer to previous work [1]. *I-V* data are obtained for PERC shingle solar cells and scaled to half-cut and full-sized solar cells for better comparability.

$$\begin{aligned} J(V) = {} & J_{\mathrm{ph}} - J_{01}\left(\exp\left\{\frac{e(V+JR_{\mathrm{s}})}{k_{\mathrm{B}}Tn_{01}}\right\} - 1\right) \\ & - J_{02}\left(\exp\left\{\frac{e(V+JR_{\mathrm{s}})}{k_{\mathrm{B}}Tn_{02}}\right\} - 1\right) \\ & + J_{\mathrm{Br}}\exp\left\{-\frac{e(V+JR_{\mathrm{s}}-V_{\mathrm{Br}})}{k_{\mathrm{B}}Tn_{\mathrm{Br}}}\right\} - \frac{V+JR_{\mathrm{s}}}{R_{\mathrm{p}}} \end{aligned} \quad (1)$$

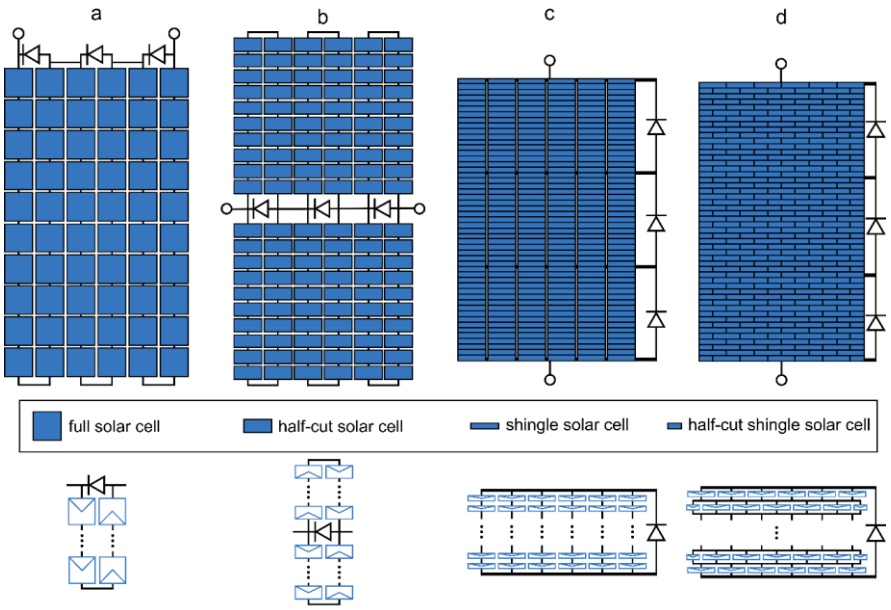

Figure 1: Module layouts investigated in LTspice shading simulations taken from [1]: a) conventional topology full-sized solar cell interconnection b) "butterfly" topology for half-cut solar cell c) shingle string and d) shingle matrix topology for shingle solar cells. For the latter a half-cut shingle solar cell is added in every second row. The electrical interconnection schemes of the different topologies within one string or block, secured by a bypass diode, are given in the bottom.

2.2 Module Layouts

Figure 1 shows a schematic drawing of the four investigated module layouts.

a) The conventional layout for full-size solar cells containing 60 solar cells, divided into strings of 10 solar cells. Two strings are interconnected in series and are bypassed by one diode each. 20 solar cells are in serial interconnection as suggested by the interconnection scheme given in the bottom part of **Figure 1**.

b) Half-cut solar cells are assembled in the so called "butterfly" layout. The upper and the lower block of solar cells are interconnected in parallel. Each block contains again three strings with a bypass-diode each. Note that each bypass-diode is in parallel to a string of the upper and the lower block. When in its conductive state at around -0.4 V both strings are bypassed.

c) The shingle string interconnection contains 6 parallel interconnected strings of 50 solar cells each. Three bypass-diodes split the strings into pieces of $16, 17$ and 17 solar cells. Note, that in a real PV solar module, there would be three times 17 thus 51 solar cells, since overlapping of the solar cells allows for additional solar cells on the same area. However, for better comparability, all simulations contain the identical number of full-cell equivalents.

d) The shingle matrix interconnection features an additional lateral overlap of the solar cells. From these results an intrinsic serial and parallel interconnection of each solar cells to its direct neighbours. Note that this requires half-cut shingle solar cells in each second row to form a rectangular active area. Similar to the string interconnection three bypass diodes split the module containing 50 solar cells in the direction of serial interconnection. In an earlier publication we showed that this scheme allows lateral current transport along the joints formed by busbars and electrically conductive adhesives (ECA). These electrode bridges allow the currents to flow past shaded areas and thus reduce the losses due to shading significantly [7].

2.3 Shading Scenarios

We consider two basic cases: rectangular and random shading. Both are shown in **Figure 2** along with exemplary irradiation maps for each case on the right side. Although shading is never absolute and *e.g.* in case of a leafy tree shaded areas are still illuminated with $\sim 200\ \mathrm{W/m^2}$ [9], for better comprehensibility we assume $0\ \mathrm{W/m^2}$ on shaded areas. In case of rectangular shading, the shaded areas are computed as precisely as the machine error. In case of random shading, we use a pixel-based approach to create random shading patterns. Both will be explained in more detail.

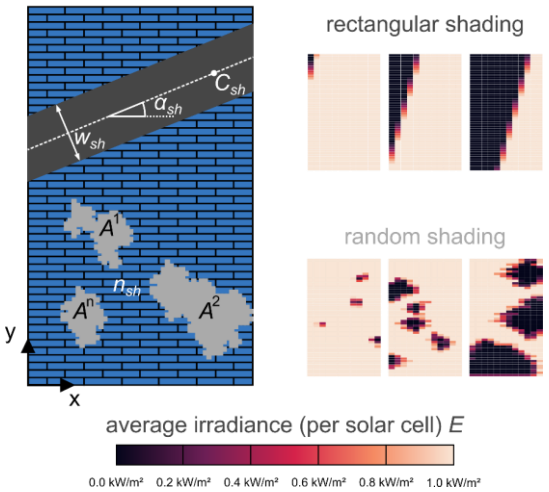

Figure 2: Left: Shading cases: rectangular and random shading. Rectangular shading is defined by three parameters width w_{sh}, angle towards the x-axis α_{sh} and the position of the rotation center C_{sh}: $(x|y)$. Random shading is defined by the shaded area fraction $A_{\mathrm{sh}} = \sum A^{\mathrm{n}}$. Right: Exemplary irradiation maps for both cases based on which the photocurrent of each solar cell is computed and passed to the LTspice circuit simulation. Irradiation levels refer to the average irradiation on one solar cell.

Rectangular shading is defined by three respectively four parameters: The shading width w_{sh}, the angle towards the x-axis α_{sh} and the rotation center C_{sh} given by its x and y coordinate. Perpendicular to the shading width the shadow expands infinitely. We compute the exact shaded area of each solar cell. According to findings of V. Quaschning [10] there is only a small error of ~2% on the MPP of a solar cell, when neglecting the spatial distribution of the irradiation and taking into account only the average irradiation on the solar cell surface. We use this finding to set the photocurrent density of a shaded solar cell $J_{\mathrm{ph,s}}$ according to its shaded area fraction A_{sh} and fractional irradiation $\hat{\imath}$ by Eq. (2).

$$J_{\mathrm{ph,s}} = J_{\mathrm{ph,0}} A_{\mathrm{sh}} (1 - \hat{\imath}) \tag{2}$$

$J_{\mathrm{ph,0}}$ is the photocurrent density measured under Standard Test Conditions (STC) ($25\,°\mathrm{C}, AM1.5, 1000\,\mathrm{W/m^2}$). A_{sh} is given by the ratio of shaded area A to entire area A_0, thus $A_{\mathrm{sh}} = A/A_0$. $\hat{\imath}$ is defined similarly as the irradiation on shaded areas E divided by the irradiation on illuminated areas I_0, thus $\hat{\imath} = E/E_0$.

Random shading is defined only by A_{sh} which is distributed on 1 to n_{sh} individual and randomly shaped areas. n_{sh} thereby defines the maximum number of shaded areas and thus is somewhat in between a parameter and a random quantity. When creating the shading scenarios, the number of shading patches is randomly chosen between $1 \ldots n_{\mathrm{sh}}$ according to the boundary value n_{sh}. A_{sh} is then distributed randomly on the shading patches. Starting from a shadow seed pixel randomly chosen on the module area, each shaded area A^{i} is built pixel by pixel. We use $25x25$ pixels per solar cell. Exemplary irradiation maps for both base cases are given in **Figure 2**. The color code refers to the average irradiation on the individual solar cells. Note that in **Figure 2** the individual solar cells, not the pixels per solar cell are displayed.

2.4 Shading Resilience

In prior work we defined a factor called the Shading Resilience SR quantifying the ability of a PV module to minimize the partial shading losses. For a more detailed explanation to the derivation of SR we refer to our publication [1].

In **Figure 3** we show the graphical definition of SR. The PV module power is given dependent from A_{sh}. The dotted lines define the minimum possible power output thus for $A_{\mathrm{sh}} = 1$. Naturally this value depends on the irradiation of the shaded areas and therefore $P_{\mathrm{min}} = \hat{\imath} P_0$ with the initial unshaded power output P_0. The core aspect is the definition of the upper physical limit for the power output under partial shading. The limit functions are given by solid lines. They represent a hypothetical parallel interconnection of all solar cells in the PV solar module. Since in parallel interconnections there is no current mismatch. Assuming ideal interconnection, the solar cells operate almost independently from each other and only the power of the shaded solar cells is lost. This defines an upper physical limit for the power output. Any possible maximum power point for any shading scenario is found between these two limiting functions. A PV module obviously incorporates a higher SR the closer it approaches P_{lim}.

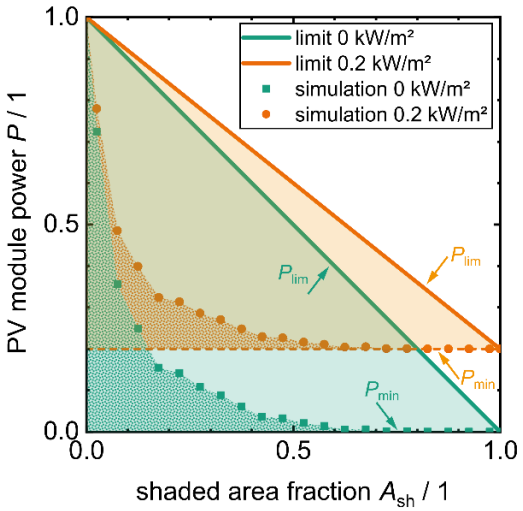

Figure 3: Graphical definition of the shading resilience according to [1]. SR is defined as the ratio of the spotted to the filled areas for two cases of $\hat{\imath} = [0; 0.2]$. The data points are a result of the simulations from the power function $P(A_{\mathrm{sh}})$.

To create common and comparable ground, we define SR as the ratio of two areas: first, the area enclosed by a power function $P(A_{\mathrm{sh}})$ and P_{min}. Second, the area enclosed by P_{lim} and P_{min}. $P(A_{\mathrm{sh}})$ is obtained in circuit simulations based on LTspice with an adequate number of data points from $A_{\mathrm{sh}} = 0$ to 1. The area below $P(A_{\mathrm{sh}})$ is obtained by integration with the trapezoidal rule. This graphical definition of SR is also given by Eq. (3). Again for more details we refer to our previous work [1].

$$SR = \frac{2}{(1-\hat{\imath})P_0} \int_0^1 P \, dA_{\mathrm{sh}} - \frac{2\hat{\imath}}{1-\hat{\imath}} \tag{3}$$

2.5 LTspice Simulations

As discussed in the previous section, we used LTspice to obtain $P(A_{\mathrm{sh}})$. Therefore, the equivalent circuit model of the (extended) two-diode model was implemented in a python code creating the netlist for LTspice. Each solar cell is represented by two virtual sub-cells. This is necessary to adequately represent the shingle matrix interconnection where the solar cells overlap laterally on half of their length. In previous work, we discussed this approach and the non-ideal current transport properties of this lateral interconnection [7]. Lateral resistors with absolute values R_{lat} interconnect the solar cells in the shingle matrix layout. For comparability, we transfer the virtual sub-cell concept on all topologies. Values of R_{lat} measured in [7] are also used in this study. We conducted validation experiments and found experimental and computed values to deviate approximately by 2 % over various shading scenarios [7].

3 SIMULATION STUDY

In the last section we introduced the components needed to obtain the shading resilience of varying module topologies. The last missing component is the power function $P(A_{\mathrm{sh}})$ for both basic shading cases. The entire process flow from the generation of input to postprocessing and obtaining SR is summarized in **Figure 4**.

We performed parameter studies based on Latin

Hypercube Sampling (LHS) [11], a method to randomly but uniformly cover a multidimensional parameter space.

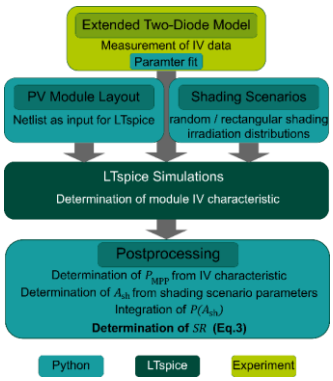

Figure 4: Flowchart of the process performed to obtain the shading resilience SR for different module layouts and basic shading cases (rectangular and random). The color code represents the software or experiment used for each step.

Therefore, each parameter is split in equidistant steps between given boundaries where the step size is defined by the chosen number of scenarios. LHS then generates random combinations of all parameters so that each step occurs exactly once.

For rectangular shadings there are four input parameters: w_{sh}, α_{sh} x and y. Their boundary values are given in **Table 1**. A_{sh} is then computed for each individual parameter set. We chose 2000 scenarios, from which 777 result in a shaded area fraction of 1. From the remaining scenarios computed in LTspice the power function $P(A_{\mathrm{sh}})$ is obtained.

Table 1: Boundaries of the parameters defining the rectangular shading scenarios

Parameter	Lower limit	Upper limit
x / mm	0	$l_{\mathrm{M}} = 1567.5$
y / mm	0	$w_{\mathrm{M}} = 940.5$
α_{sh} / °	0	90
w_{sh} / mm	0	$2\sqrt{l_{\mathrm{m}}^2 + w_{\mathrm{M}}^2} = 3656.0$

In case of random shading there is only one parameter: A_{sh}. We adjusted the number of computations to rectangular shading. Thus 1250 random scenarios form $P(A_{\mathrm{sh}})$ in equidistant steps from $A_{\mathrm{sh}} = 0$ to 1 for random shading.

4 RESULTS AND DISCUSSION

Table 2 summarizes the obtained values for the shading resilience of all module layouts and both basic shading cases. We emphasize, that due to the large number of computed scenarios and the capability of LHS to represent multidimensional parameter spaces the SR values feature a very high significance. As mentioned before, SR can be interpreted as the share of the ideal shading resilient module layout: A parallel interconnection of all solar cells. Thus, the results show that *e.g.* a shingle matrix module under any possible rectangular shading yields close to 70 % of the maximum possible power, while *e.g.* the conventional layout can only generate ~20 %. Hence, in average there is a factor of ~3.5 in the power output under rectangular shading.

Table 2: Shading resilience computed for all module topologies and both basic shading cases.

Module Layout	SR rectangular	SR random
Shingle Matrix	0.692	0.545
Shingle String	0.602	0.446
Butterfly	0.461	0.319
Conventional	0.213	0.207

We find similar results for random shading. However, the absolute values of SR are reduced by $\Delta SR = 15\ \%_{\mathrm{abs}}$ compared to rectangular shading for all module layouts. This is explained by the fact that rectangular shading covers distinct parts of the solar module, which in consequence can be bypassed. Random shading on the other hand is very likely to distribute on the entire surface. Thus, all bypassed substrings are likely to be affected equally. Since besides the conventional layout all others incorporate parallel interconnected solar cells, they are affected more by this resulting in the above-mentioned differences. The conventional layout however has very few cases in which only one or two strings are affected by shading after all.

To further investigate reasons for the differences in SR we show *I-V* data of all topologies in **Figure 5**. Each plot shows the currents at the MPP on the left y-axis (colored data) and the voltage at the MPP on the right y-axis (grey data). On the x-axis the shaded area fraction is shown. In the left column the results for rectangular, in the right column the results for random shading are shown. Please note, that there are slight differences in the I_{sc} and V_{oc} between the shingle and the other two topologies which is due to the fact, that we used 1/5$^{\mathrm{th}}$ shingle solar cells. This leads to slightly higher currents at lower voltages in the shingle modules. First and most prominent difference is the fact, that both shingle module topologies produce currents over the whole range of A_{sh} from 0 to 1. The half-cell butterfly and the full cell conventional layout on the other hand show a distinct threshold at $A_{\mathrm{sh}} \cong 0.9$ and $A_{\mathrm{sh}} \cong 0.8$, respectively, where currents drop to 0. For rectangular shading this threshold is located at $A_{\mathrm{sh}} \cong 0.7$ and $A_{\mathrm{sh}} \cong 0.3$, respectively. This again is caused by the fact, that for a concentrated, rectangular shading it is more likely to affect all strings, while it takes a larger area of randomly shaped, distributed shading to achieve the same effect.

All graphs show distinct horizontal lines in the I_{MPP} data. They correspond to states with active bypass diodes or in case of the butterfly layout at ~4.5 A to a fully illuminated module half. They illustrate how bypass diodes even for large shaded area fractions enable the extraction of the unshaded I_{MPP} current from the solar modules. This becomes especially important, when many modules are interconnected in power plant applications and the individual module MPP becomes less important than the global module string MPP. Again, both shingle topologies show significant more data points at the unshaded I_{MPP} compared to the butterfly and conventional layout. These data points are found even for values of $A_{\mathrm{sh}} > 0.5$ where both butterfly and conventional layout in most of the cases are at zero current already.

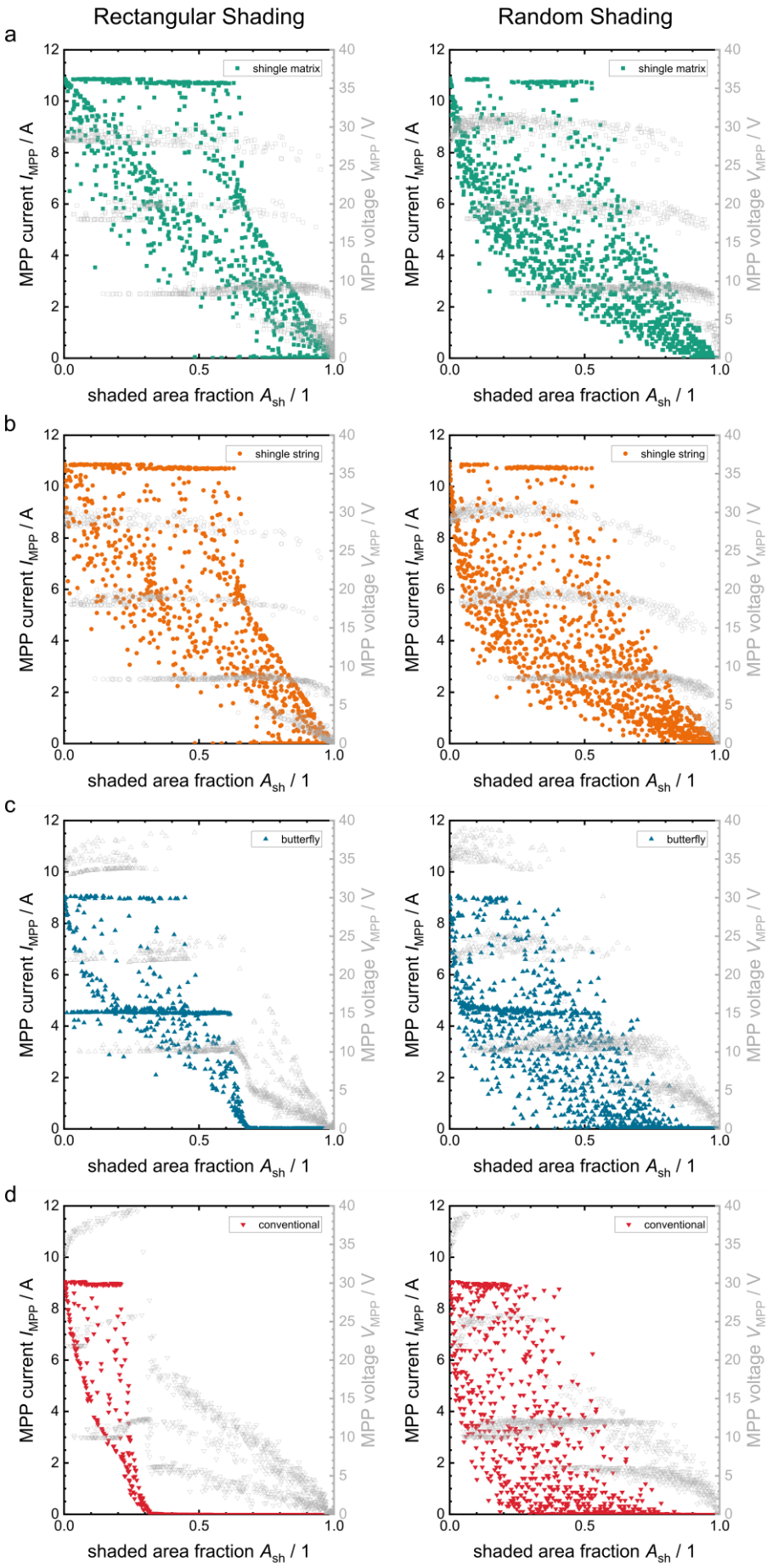

Figure 5: Diagrams of the I_{MPP} and V_{MPP} dependent from the shaded area fraction A_{sh}. The left y-axis shows $I_{\mathrm{MPP}}(colored\ data)$, the right y-axis shows the V_{MPP} values (grey data). **a** to **d** correspond to the different module layouts: a) shingle matrix, b) the shingle string, c) the half-cell butterfly and d) the conventional full cell topology. While currents distribute over the entire range from 0 to the unshaded I_{MPP} the V_{MPP} data points form distinct clusters corresponding to the number of conductive bypass diodes. Horizontal lines in the current data also indicate states of conductive bypass diodes or in case of the butterfly module at ~4.5 A one fully operational half of the module.

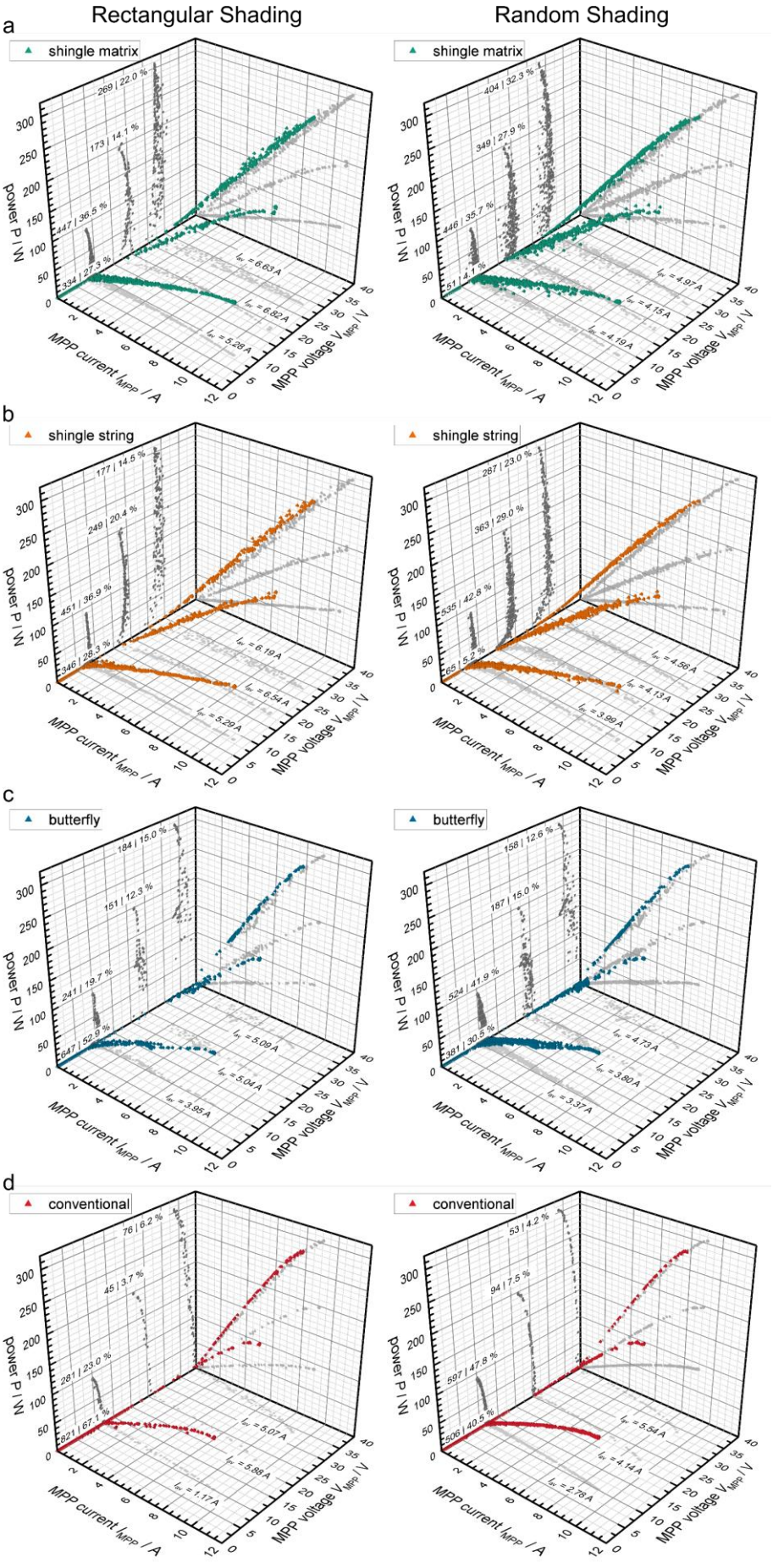

Figure 6: 3D plot of the I_{MPP} and V_{MPP} data shown in **Figure 5**. Additionally, the module power is given on the z-axis. It becomes visible that the data points form distinct groups again correspond to the different states of conductive bypass diodes. For each group the absolute number of data points and percentage of all scenarios are shown on the yz-projection plane. On the xy-projection plane the average current of each group is added.

Figure 6 shows three-dimensional plots of the I_{MPP} and V_{MPP} data from **Figure 5**, adding the module power on the z-axis. In all cases the data show three respectively four distinct groups. The first three represent the different configurations of conductive bypass diodes. The fourth group corresponds to the data points found at zero currents. For all groups absolute numbers of data points and percentages from the entire set of scenarios are shown on the yz-projection plane. In the same way, the xy-projection plane incorporates the average MPP currents I_{av} for all groups. We use the V_{MPP} values to group the data points. For the shingle modules we use 5 V to 15 V, 15 V to 25 V and 25 V to 35 V. For butterfly and conventional layout, we use 10 V to 20 V, 20 V to 30 V and 30 V to 40 V.

We find the before mentioned differences confirmed, especially with respect to current extraction and number of states without conductive bypass diodes. As an example, the groups with no conductive bypass diodes are examined: for the shingle matrix it contains 22.0 % of the data with an average MPP current of 6.63 A. The shingle string contains 14.5 % of the data at $I_{\mathrm{av}} = 6.19$ A. The butterfly slightly exceeds the shingle string with 15.0 % of the data. However, its I_{av} is at 5.09 A. The conventional layout only in 6.2 % of the cases is without conductive bypass diodes and has $I_{\mathrm{av}} = 5.07$ A.

Random scenarios in general lead to more cases without conductive bypass diodes. Again, this is caused by the distribution of shading on the entire surface leading to less mismatch between bypassed regions.

5 CONCLUSIONS

In this work we present results of partial shading simulations based on an extended two diode model with reverse bias characteristics. We compared four different module layouts: Two modules with shingle solar cells, a half-cut solar cell module with butterfly layout and a conventional solar module with full-sized cells. Rectangular and random shading have been examined to cover the shading by pylons or chimneys and the shading by leaves or bird droppings. We calculated > 1000 scenarios each. From the obtained data, we evaluated the shading resilience SR of the module as defined in [1]. For rectangular and random shading, the shingle modules exceed the half-cell butterfly and the full cell modules significantly. We find the highest values for SR under rectangular shading with $SR = 0.692$ for the shingle matrix, $SR = 0.602$ for the shingle string, $SR = 0.461$ for the butterfly and $SR = 0.213$ for the conventional layout. This means that *e.g.* in any rectangular shading scenarios the shingle matrix module has in average a factor 3.5 $(0.692/0.213)$ higher power output compared to the conventional layout. The large parameter space in combination with Latin Hypercube Sampling ensures a high significance of the obtained SR values.

In random shading scenarios, SR is reduced for all module topologies. This is explained by the distribution of shading on the entire solar module surface, lowering the overall module current which can be seen by comparing the average currents, *e.g.* for the shingle matrix module 6.63 A for rectangular vs. 4.97 A for random shading. Similar differences are found for all other topologies.

In conclusion, shingle solar modules offer a generally increased resilience to partial shading. In both rectangular and random shading cases they are closer to the ideal shading resilient solar module layoutlayout - a parallel interconnection of all solar cells - than the half-cell or full cell topologies. This makes modules with shingle solar cells especially suited for integrated applications such as VIPV and BIPV. Future work aims to not only show the advantage in power output, but also energy yield by outdoor yield experiments under varying partial shading situations.

6 ACKNOWLEDGEMENTS

The authors thank all colleagues from Fraunhofer ISE who contributed to this work and namely Heinz Riesch-Oppermann from KITs IAM-WBM for fruitful discussions on sampling and statistics. This work was supported by the German Federal Ministry for Economic Affairs and Energy (BMWi) under the contract number 03EE1026A, acronym Shirkan. We also thank the German Federal Environmental Foundation (DBU) for supporting our research within their graduate scholarship program.

6 REFERENCES

[1] N. Klasen, F. Lux, J. Weber, T. Roessler, and A. Kraft, “"Shading Resilience" as a General Measure of Shading Tolerability in PV Modules,” *IEEE Journal of Photovoltaics*, tbp.

[2] U. Jahn and W. Nasse, “Operational performance of grid-connected PV systems on buildings in Germany,” *Prog Photovoltaics*, vol. 12, no. 6, pp. 441–448, 2004, doi: 10.1002/pip.550.

[3] C. Schuss, B. Eichberger, and T. Rahkonen, “Impact of solar radiation on the output power of moving photovoltaic (PV) installations,” in *2018 IEEE International Instrumentation and Measurement Technology Conference (I2MTC)*, Houston, TX, May. 2018 - May. 2018, pp. 1–6.

[4] C. Schuss, T. Kotikumpu, B. Eichberger, and T. Rahkonen, “Impact of dynamic environmental conditions on the output behaviour of photovoltaics,” in pp. 993–998.

[5] Deutsche Gesellschaft für Sonnenenergie, *Planning and installing photovoltaic systems: A guide for installers, architects and engineers*, 3rd ed. London: Routledge Taylor & Francis Group, 2013. [Online]. Available: http://site.ebrary.com/lib/hawhamburg/docDetail.action?docID=10737858

[6] D. Götz, D. Hahn, R. Gottschalg, D. Dassler, S. Schindler, and H. Hanifi, “Evaluation of Shading Tolerance of PV Modules with different Module Designs for mobile Applications by Simulation, indoor and outdoor Measurements,” in *Proceedings of the 36th European Photovoltaic Solar Energy Conference and Exhibition*, Marseille, France, 2019.

[7] N. Klasen, D. Weißer, T. Geipel, D. H. Neuhaus, and A. Kraft, “Performance of Shingled Solar Modules Under Partial Shading,” *Progress in Photovoltaics: Research and Applications*, tbp.

[8] H. S. Rauschenbach, *Solar cell array design handbook: The principles and technology of*

photovoltaic energy conversion. New York: Van Nostrand Reinhold Co, 1980.

[9] M. A. Sattler and S. Sharpies, “FIELD MEASUREMENTS OF THE TRANSMISSION OF SOLAR RADIATION THROUGH TREES,” in *Advances In Solar Energy Technology*: Elsevier, 1988, pp. 3846–3850.

[10] V. Quaschning, “Simulation der Abschattungsverluste bei solarelektrischen Systemen,” Dissertation, Technische Universität Berlin, Berlin, 1996.

[11] M. D. Mckay, R. J. Beckman, and W. J. Conover, “A Comparison of Three Methods for Selecting Values of Input Variables in the Analysis of Output from a Computer Code,” *Technometrics*, vol. 21, no. 2, p. 239, 1979, doi: 10.2307/1268522.